THE UNIVERSITY OF TEXAS AT DALLAS
McDermott Library

TREASURES
@UT Dallas

Erik Jonsson School of Engineering and Computer Science

On the Permeability of Colloidal Gels

UT Dallas Author(s):

Lev D. Gelb

Lev D. Gelb ⓘD, Alan L. Graham, Alex M. Mertz, and Peter H. Koenig ⓘD

COLLECTIONS

^{EP}   This paper was selected as an Editor's Pick

View Online   Export Citation   CrossMark

ARTICLES YOU MAY BE INTERESTED IN

On the permeability of colloidal gels

Lev D. Gelb,[1] Alan L. Graham,[2] Alex M. Mertz,[2] and Peter H. Koenig[3]

AFFILIATIONS

[1] Department of Materials Science and Engineering, University of Texas at Dallas, Richardson, Texas 75080, USA

[2] Department of Mechanical Engineering, University of Colorado—Denver, Denver, Colorado 80204, USA

[3] Procter and Gamble, Beauty Care Modeling and Simulation, Sharon Woods Innovation Center, 11511 Reed Hartman Highway, Cincinnati, Ohio 45241, USA

ABSTRACT

We reexamine and refine analytical theories for permeability in colloidal networks, with particular focus on constants and identification of approximations. The new theories are compared against numerical simulations of Stokes flow through the networks and reveal nearly quantitative power-law predictions for both pore size and permeability at low volume fractions, with systematic deviations observed only at high volume fractions. Comparison with two previously published experimental data sets yields mixed results: in one case, very good agreement is found, while in the other, only the scaling is correctly predicted. In fractal gel networks, the permeability is commonly modeled as a power-law function of volume fraction, with the fractal dimension of the network determining the power-law exponent. To quantitatively probe the influence of gel structure on permeability, we investigate this relation in structures generated by diffusion-limited cluster aggregation (DLCA) and reaction-limited cluster aggregation (RLCA) and, for contrast, non-overlapping uniform random dispersions of particles. Geometric analyses are used to determine network pore size distributions, fractal dimensions, and percolation characteristics. High-fidelity simulations of the slow viscous flow of Newtonian fluids are used to obtain first-principles-based velocity and fields and hence network permeabilities. Interestingly, the effective pore size that determines permeability is found to be somewhat larger than that measured by a method based on the insertion of spherical probes. Empirical inclusion of a fractal dimension dependence on volume fraction is found to yield quantitative results for permeabilities over the entire volume fraction range studied, in both DLCA and RLCA materials.

Published under license by AIP Publishing. https://doi.org/10.1063/1.5054596

I. INTRODUCTION

Colloidal gels are self-assembled particle networks that form space-spanning structures.[1] These systems have commercial applications in tissue engineering, drug delivery, and a remarkably broad range of consumer products.[2-10] Colloidal gels display a wide range of topology, ranging from fractal agglomerates[11] to structures composed of dense strands of particles,[12] depending on the volume fraction occupied by the particles, ϕ, and the strength and character of the interparticle interactions. Particles interacting through strong and short-ranged interactions tend to form fractal structures, while softer interactions that allow for a rapid reorganization of local structure lead to structures of much higher local coordination that coarsen with time (spinodal decomposition-like behavior); these phenomena have been thoroughly reviewed.[13]

The structure of colloidal gels can be probed by light scattering,[14] confocal microscopy,[12,15] and other techniques. In fractal networks, the fractal dimension d_f is the most critical structural parameter and determines how network mechanical and transport properties scale with volume fraction. As the gel forms, interparticle bonding leads to small aggregates, which further agglomerate to form a gel: a network that spans the entire system.[1,16-19] The fractal dimension is determined by the physics of the aggregation process that produces the network structure; if particles bond upon first contact, then "diffusion-limited cluster aggregation" (DLCA) networks form, while if a kinetic barrier prevents bonds from forming in most collisions, then one obtains "reaction-limited cluster aggregation" (RLCA) structures, with different fractal dimensions. The structure of fractal gels is homogeneous on large length scales and controlled by packing considerations at very small length scales; fractal behavior is observed over an intermediate

range, up to a few times the mean pore size.[20,21] Limited coarsening and restructuring occurring during aggregation may not have a substantial effect on the fractal dimension but can significantly change gel mechanical properties.[22]

Suspensions and emulsions are a common motif in consumer products, and they are used to deliver particles or liquid droplets through dispersion in a carrier medium. Non-neutrally buoyant particles have an equilibrium state as loose sediment at the bottom (or top) of their container. However, if attractive interparticle forces are present, particles can form network structures which can resist collapse. If the network modulus is large, then these networks can be stable for long time scales. If the network is insufficiently strong, then a period of slow initial compression or delayed sedimentation is observed, followed by a rapid collapse and a final period of slow further compression.[23–26] The rate of initial compression is determined by the permeability of the gel network, that is, the rate at which the surrounding solvent can be transported through the collapsing gel. This relationship has been used to measure gel permeabilities.[23,27,28] Gels with lower permeability are stable over longer time scales than gels of higher permeability, and controlling permeability is therefore critical in gel-stabilized product and application designs where there is little tolerance for settling.

Quantitative understanding of the permeability of high-porosity materials is lacking. While there is a large literature on the permeability of porous matrices,[29,30] most work in this area has concerned relatively low-porosity (high volume fraction) materials, especially geological materials[30–33] with applications in oil and gas extraction[34] and aquifer management.[35] High-porosity materials are widely used in chromatography (e.g., gel electrophoretic separation of proteins[36,37]), but the focus in the study of these systems is the transport coefficients of large molecules moving through the gel network. Prior studies[23,27] have proposed scaling relations which show that the permeability varies with volume fraction according to a function of the fractal dimension d_f, but these relations, as shown below, are not suitable for quantitative prediction. Scaling theories are also likely to be unreliable for high-volume fraction networks with very small pores, since fractal behavior does not extend down to the smallest length scales. Finally, scaling theories have not been extended to the networks of high aspect-ratio particles and particle mixtures that appear in commercial applications. As a result, attempts to engineer colloidal network systems are almost entirely empirical.

In this study we use large-scale simulations to investigate the relationships between network structure and permeability in different gel structures. Gel models are generated by off-lattice DLCA and RLCA simulations, with "non-overlapping uniform random" (NOUR) particle dispersions used as an additional reference. These microstructures serve as boundary conditions for high precision Stokes flow simulations that determine network permeabilities from first principles. These permeabilities are then used to evaluate previously proposed scaling relations and new quantitative predictions for fractal gel permeability.

We first review the derivation of scaling theories that relate the effective pore size in the networks to the size of the fractal clusters of which they are composed. We identify the various approximations involved and extend this approach to generate quantitative predictions of pore size based on various assumptions. The pore size models are then combined with flow models based on the assumption of locally cylindrical pores to provide predictions of gel permeability. Predictions of both pore size and permeability are critically evaluated by comparison with pore size distributions and permeabilities obtained from computer simulations. Empirical models for permeability that involve ϕ-dependent fractal dimensions are then considered. Finally, the derived permeability predictions are applied to available experimental data.

II. THEORY

A. Cluster spacing and pore size

Carpineti and Giglio[14] derived a scaling relation for cluster spacing in DLCA networks based on a physical picture whereby fractal clusters grow until "all the available space is filled with closely packed clusters,"[14] at which point one has formed a system-spanning network. This accounts for the observed crossover from fractal structure at smaller length scales to homogeneous behavior at large length scales; for lengths much larger than the average cluster size, the structure should be uniform if it consists of such closely packed clusters. We re-derive this scaling relation here, paying careful attention to implicit assumptions and treatment of constant factors. It is well established that in diffusion-limited aggregation, the number of primary particles contained within a large cluster varies with its radius R_c according to $N_c \propto R_c^{d_f}$, where d_f is the fractal dimension.[18,19] Based on this, we take the number of particles in a cluster as given by

$$N_c = \left(\frac{R_c}{a}\right)^{d_f} = \left(\frac{D_c}{2a}\right)^{d_f},\qquad(1)$$

where the cluster diameter $D_c = 2R_c$ and a is the constituent particle radius, assumed monodisperse. This result is an approximation, obtained by assuming both that fractal behavior persists all the way down to the single-particle limit, such that $N_c = 1$ when $D_c = 2a$, and that clusters of a given radius all contain the same number of particles.

If n_0 is the monomer (particle) number density, then the cluster number density is $n_c = n_0/N_c$; the volume per cluster is then $V/N_c = 1/n_c = N_c/n_0$, where V is the total volume of the system. In order to relate the volume fraction to the inter-cluster distance and thus the cluster diameter, one must assume some packing model for the clusters. Previous analyses[14,17] have set the volume per cluster equal to the cluster diameter cubed, that is, $V/N_c = D_c^3$. This is equal to the volume fraction for simple-cubic packing, with a "cluster packing fraction" $\phi_c = \pi/6 \simeq 0.524$. This is not to say that previous analyses claimed that the clusters were actually arranged in a cubic lattice, but only that their actual arrangement had an equivalent volume fraction. Alternative possibilities might be

true close-packing, with $\phi_c \simeq 0.74$, random close-packing, with $\phi_c \simeq 0.64$, or the packing of loosely settled spheres, $\phi_c \simeq 0.44$.[29] Whatever the packing model chosen, the volume per cluster is then the actual volume occupied by the cluster divided by the packing fraction,

$$\frac{V}{N_c} = \frac{4\pi}{3} R_c^3 \cdot \frac{1}{\phi_c}. \tag{2}$$

Combining this with Eq. (1), etc., gives

$$R_c^3 = \left(\frac{N_c}{n_0}\right) \cdot \frac{\phi_c}{4\pi/3} = \frac{1}{n_0} \left(\frac{R_c}{a}\right)^{d_f} \cdot \frac{\phi_c}{4\pi/3} \tag{3}$$

and after collecting powers of R_c,

$$R_c^{3-d_f} = \frac{1}{n_0} \cdot \frac{1}{a^{d_f}} \cdot \left(\frac{\phi_c}{4\pi/3}\right). \tag{4}$$

Likewise, the number density of particles is related to the volume fraction of particles, ϕ, by

$$n_0 = \frac{3}{4\pi} \cdot \frac{\phi}{a^3}. \tag{5}$$

Inserting this into Eq. (4), collecting powers of a, and rearranging gives

$$\left(\frac{R_c}{a}\right)^{3-d_f} = \frac{1}{\phi} \cdot \phi_c, \tag{6}$$

and, finally, the cluster diameter and radius in units of particle radius are

$$\frac{D_c}{a} = \frac{2R_c}{a} = \left[2\phi_c^{\frac{1}{3-d_f}}\right] \cdot \phi^{\frac{1}{d_f-3}}. \tag{7}$$

The cluster diameter thus varies with particle volume fraction according to a power law with exponent $1/(d_f - 3)$, independent of the choice of the cluster packing model. The prefactor (term in brackets) does depend on the choice of the packing model, but is always close to unity. For example, choosing $d_f = 1.83$ (as used below) and $\phi_c = 0.44$ yields a prefactor of 0.991, while $d_f = 1.83$ and $\phi_c = \pi/6$ give 1.150. Increasing the fractal dimension decreases the value of the prefactor; for RLCA-like $d_f = 2.1$ and $\phi_c = 0.44$ the prefactor is 0.803.

The cluster size is strongly dependent on the fractal dimension; changing d_f even from 1.9 to 2.0 at $\phi = 0.01$ increases the cluster size by a factor of 1.5, and changing from 1.9 to 2.1 increases it by a factor of 2.5.

To relate the pore size to the cluster size requires further approximation. Manley et al.[23] assumed that the diameters of channels through the gel network are *equal* to the fractal cluster diameter, $D_{pore} = D_c$, and dropped all prefactors, leading to

$$\frac{D_{pore}}{a} = \phi^{\frac{1}{d_f-3}}. \tag{8}$$

Alternatively, we can keep the prefactors, which we refer to as the "cluster model" prediction,

$$\frac{D_{pore}}{a} = \frac{D_c}{a}. \tag{9}$$

There are other options for relating the cluster size to the channel size. The "hydraulic" approximation, used in studies of flow in packed beds, is to choose an effective cylindrical pore diameter that preserves the surface area per volume of the actual material;[29] for a bed of spheres of diameter D_c at volume fraction ϕ_c, the result is that the pore diameter $D_{pore} = 2D_c/3 \cdot ((1 - \phi_c)/\phi_c)$. Applying this to the fractal cluster model yields the following "hydraulic model:"

$$\frac{D_{pore}}{a} = \frac{2}{3}\left(\frac{1 - \phi_c}{\phi_c}\right) \cdot \frac{D_c}{a}. \tag{10}$$

Here the pore size also varies with particle volume fraction according to a power law with exponent $1/(d_f - 3)$, again independent of the choice of the cluster packing model, but with a different prefactor than before. For example, choosing $d_f = 1.83$ (as used below) and $\phi_c = 0.44$ now yields a prefactor of 0.841, while choosing $d_f = 1.83$ and $\phi_c = \pi/6$ gives 0.697, both of which are smaller than the corresponding prefactors in the "cluster" model.

B. Permeability of a material consisting of parallel cylindrical pores

Next we assume that flow through the gel can be modeled as a bulk material penetrated by non-interacting cylindrical pores aligned along the flow direction. The Hagen-Poiseulle model for flow in a single cylinder of diameter D is

$$Q_{HP} = \frac{dP}{dz} \frac{\pi D^4}{128\mu}. \tag{11}$$

Darcy's Law is

$$Q = k_0 \frac{A}{\mu} \frac{dP}{dz}. \tag{12}$$

In these expressions, Q is the flow in the z direction, $\frac{dP}{dz}$ is the pressure gradient in the direction of flow, μ is the viscosity of the fluid, and k_0 is the permeability. Setting these equal, canceling the derivatives, and choosing $A = \pi D^2/4$ gives

$$k_0 = \frac{\pi D^4}{128\mu} \cdot \frac{4\mu}{\pi D^2} = \frac{D^2}{32}. \tag{13}$$

This result, which only accounts for the area of the pore itself, was also obtained by Dullien.[29] The permeability of the material as a whole depends on the porosity (the volume fraction occupied by the pores). For a material of (solid) volume fraction ϕ penetrated by cylindrical pores, the porosity is $1 - \phi$. Using $A_{pore}/A_{total} = V_{pore}/V_{total} = 1 - \phi$, the total cross-sectional area of material per pore of diameter D is then $A = \pi D^2/4(1 - \phi)$, which gives

$$k_0 = \frac{D^2}{32}(1 - \phi). \tag{14}$$

If the pore diameters are not monodisperse but instead distributed according to some $f(D)$, this becomes

$$k_0 = (1 - \phi) \cdot \int f(D) \times \frac{D^2}{32} dD = \frac{1 - \phi}{32}\overline{D^2}, \tag{15}$$

where $\overline{D^2}$ is the expected value of D^2. Since the variance of the pore size distribution $\sigma_D^2 = \overline{D^2} - \overline{D}^2$, this can also be written as

$$k_0 = \frac{1-\phi}{32}\left(\overline{D}^2 + \sigma_D^2\right). \tag{16}$$

Note that this result is only applicable to the case where the pores remain perfectly cylindrical but are not all the same diameter; this analysis likewise ignores misalignment of the pores to the flow direction and branching or other network effects.

C. Models for gel permeability

Manley *et al.* assumed that the diameters of channels through the gel network are equal to the fractal cluster diameter [Eq. (8)], combined this with the D^2 dependence of k_0, and grouped all constants into a single prefactor assumed to be of order unity to obtain[23]

$$\frac{k_0}{a^2} = \phi^{\frac{2}{d_f-3}}. \tag{17}$$

For their chosen value of $d_f = 1.9$, this gives $k_0/a^2 = \phi^{-1.82}$. This prediction omits the prefactor term in the expression for the cluster diameter and the factor of $1/32$ in the expression for permeability, as well as the $1 - \phi$ due to the volume occupied by the material.

If we use the "cluster model" prediction for D_{pore} and keep all the prefactors, then combining Eqs. (7), (9), and (14) yields

$$\frac{k_0}{a^2} = \left[\frac{4}{32}\phi_c^{\frac{2}{3-d_f}}\right]\cdot\phi^{\frac{2}{d_f-3}}\cdot(1-\phi), \tag{18}$$

where the prefactor (in brackets) depends on both d_f and ϕ_c. With $d_f = 1.9$ and $\phi_c = \pi/6$, the prefactor evaluates to 0.0386, which is quite a bit smaller than 1.

If we instead choose the hydraulic model prediction for pore size, combining Eqs. (7), (10), and (14) results in

$$\frac{k_0}{a^2} = \left[\frac{4}{9}\left(\frac{1-\phi_c}{\phi_c}\right)^2 \frac{4}{32}\phi_c^{\frac{2}{3-d_f}}\right]\cdot\phi^{\frac{2}{d_f-3}}\cdot(1-\phi). \tag{19}$$

Again, the prefactor depends on both d_f and ϕ_c; in this case, with $d_f = 1.9$ and $\phi_c = \pi/6$, it evaluates to 0.0141. In Eqs. (18) and (19), the final $1 - \phi$ term will result in a small negative deviation from power-law scaling at high ϕ which is not present in the Manley model.

A reasonable question at this point is whether the final factor of $1 - \phi$, which accounts for porosity, should instead be $1 - \phi_c$. Using $1 - \phi_c$ is consistent with a physical picture where flow occurs only through the spaces *between* the fractal clusters, while using $1 - \phi$ corresponds to a picture where flow occurs through the "bodies" of the clusters as well as inter-cluster spaces. The practical effects of the $1 - \phi_c$ choice are to restore power-law behavior at even high ϕ and reduce the predicted permeability by approximately a factor of two at all volume fractions. Since the clusters themselves are highly porous, the former choice seems more reasonable and is used here; we return to this point in Sec. IV B.

Finally, note that the hydraulic approximation is one of the assumptions behind the well-known Carman-Kozeny and Blake-Kozeny models for the permeability of packed beds,[29] which are of the form

$$\frac{k_0}{a^2} = C \cdot \frac{(1-\phi)^3}{\phi^2}. \tag{20}$$

This is clearly visible in Eq. (19) if the $1 - \phi_c$ choice is made in accounting for porosity; again, this corresponds to only considering the flow between clusters. The resulting expression is essentially the Carman-Kozeny result but multiplied by a ϕ-dependent term which determines the cluster size,

$$\frac{k_0}{a^2} = \left[\frac{4}{9}\frac{(1-\phi_c)^3}{\phi_c^2}\cdot\frac{4}{32}\cdot\phi_c^{\frac{2}{3-d_f}}\right]\cdot\phi^{\frac{2}{d_f-3}}. \tag{21}$$

III. COMPUTATIONAL DETAILS

In order to critically evaluate the relationships between gel volume fraction, pore size, and permeability, we prepare model structures by simulation and then determine their various properties; the methods used are discussed in this section.

A. Model preparation

Three different types of material structures are considered in this work: gel structures resulting from a diffusion-limited cluster aggregation (DLCA) process, gel structures resulting from a reaction-limited cluster aggregation (RLCA) process, and, for contrast, structures consisting of a non-overlapping uniform random (NOUR) distribution of particles. In NOUR structures, spatial correlations are completely absent except at very small length scales, where the non-overlapping condition generates hard-sphere fluid-like behavior. All calculations are performed in cubic simulation cells with periodic boundaries in all three directions. To generate a NOUR structure, we randomly place particles in the simulation cell; if each new particle does not overlap any of the previously placed particles, the new particle is accepted; otherwise, a new position is considered. This is repeated until the desired volume fraction is achieved. To generate DLCA structures, we use a slightly modified version of the DLCA algorithm introduced by Jullien *et al.*[21,38] One starts with a NOUR configuration considered as a collection of N aggregates (clusters) containing one particle each. The system evolves in the following way: an aggregate i containing n_i particles is chosen at random according to probability p_{n_i} given by

$$p_{n_i} = \frac{n_i^\alpha}{\sum_i n_i^\alpha}, \tag{22}$$

with α being a parameter describing the effect of a cluster's size on its diffusion constant. A direction is chosen from a uniform distribution on a sphere and the cluster is moved a fixed distance δl in that direction; in this work, $\delta l = a$ (DLCA) or $1.5a$ (RLCA). If the cluster does not collide with any other cluster, the simulation continues by choosing another cluster at random and moving it. If a collision occurs, the moving cluster is

backed off until the point of contact and the two clusters are joined at that point. The process is repeated until a single cluster remains in the system. The cluster diffusion constants are made to vary as the inverse of the cluster radius by choosing $\alpha = -1/d_f$ (−0.55 in the case of DLCA simulations, for which $d_f \simeq 1.8$), though previous studies have found that the properties of the simulated gels are insensitive to the exact value used.[38]

In RLCA simulations, a similar procedure is followed except that when two particles meet, the probability of a bond being formed is only $P = 0.001$. If a bond is formed, then the two clusters are joined as in DLCA; if a bond is not formed, then the "moving" cluster is backed off to a point randomly chosen between its initial position and the position it occupied at contact. The simulation then continues by choosing and moving another cluster. For RLCA simulations, the fractal dimension is $d_f \simeq 2.1$, so α was chosen equal to −0.475.

Selected DLCA structures generated in this way are shown in Fig. 1. In this investigation, DLCA and NOUR structures were generated down to $\phi = 0.001$; RLCA structures were only generated for ϕ values of 0.003 and above, due to the much longer simulation times required; the highest volume fraction considered in all cases was $\phi = 0.25$. Calculations were run on a single core of an Intel Xeon E3-1240 V2 processor. A single DLCA simulation at $\phi = 0.01$ in a simulation cell measuring $300a$ on a side required approximately 0.48 h to complete, while a RLCA simulation under the same conditions required 7.56 h; the longest simulations run for this study (RLCA, $\phi = 0.003$, $800a$ cells) each took around 650 h. Detailed information on the system sizes used for each calculation is given in the supplementary material.

B. Model characterization

In previous studies,[40,41] we implemented a lattice-based version of a pore-size distribution calculation based on the insertion of spherical probe particles.[42,43] Briefly, one determines the volume of the void space "coverable" by spheres of radius r or smaller; a lattice site x contributes to this if and only if one can construct a sphere of radius r that overlaps x but does not overlap any gel-occupied lattice sites. This volume is a monotonically decreasing function of r. Its derivative is the fraction of the void volume characterized by a certain radius r (e.g., coverable by spheres of that radius but not larger spheres) and is a robust definition of a pore size distribution. For regular pore structures, such as a collection of spherical or cylindrical voids, this definition will simply regenerate the distribution of sphere or cylinder radii. For the off-lattice gel models studied here, the lattice representation is calculated by overlaying the gel model on a simple cubic lattice and determining which sites are covered by the gel particles. This calculation is done at different resolutions, depending on the volume fraction (and thus pore size). In general, lattices of approximately 300^3 points were used. For high volume fractions, this gave resolutions of up to 14 lattice points per particle diameter, while for very low volume fractions only 1 or 2 points per diameter were used; testing at selected ϕ with several discretizations confirmed that the resulting pore size distributions were well-converged. We also calculate the largest passable-probe diameter (LPD), also known as the "through-pore" diameter,[44] which is the size of the largest spherical probe that can pass entirely through the material and therefore defines the tightest "constrictions" in the pore network. Finally, radial distribution functions in the simulated materials were calculated using standard off-lattice methods[45] and

(a) 0.2% volume fraction

(b) 0.5% volume fraction

(c) 1.0% volume fraction
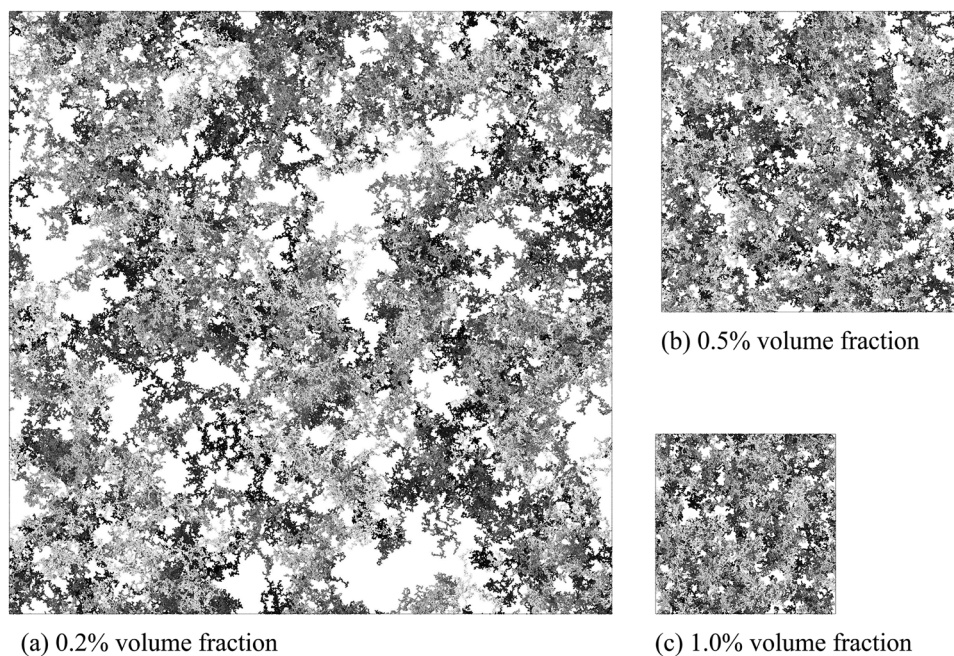
FIG. 1. DLCA aerogel structures at 0.2%, 0.5%, and 1.0% gel volume fraction. Particles are shaded by depth, with those at the front of the simulation cell in white and those at the back in dark gray. The size of the simulation cell necessary to contain a statistically significant sample of the gel structure depends on the volume fraction; these cells measure 500^3, 250^3, and 150^3 particle diameters, respectively. Figure adapted from Ref. 39.

used to determine fractal dimension in low-density models, as described below. All structural data reported are averages over 15 separate simulations at the stated conditions; uncertainties were calculated from the standard deviation as $\pm 2\sigma/\sqrt{15}$.

C. Permeability calculations

Here we focus on the slow flow of a Newtonian fluid through the colloidal network. Under these conditions, the pore Reynolds number is very small and the Stokes equations are very good approximations to the full Navier-Stokes equations. Hence accurately solving the Stokes equations provides a numerically "exact" solution to flow of the fluid in the colloidal network.[46]

These principles are well known but until recently both analytical and numerical limitations have limited the availability of exact solutions to relatively small systems. In this work, we capitalize on recent numerical advances that have dramatically increased the speed and accuracy of Stokes flow simulations, enabling the solution of flow problems in networks containing very large numbers of particles. Permeabilities were calculated in the commercial software package GeoDict.[44] GeoDict implements an extremely fast LIR-tree based adaptive-grid solver on a simple cubic mesh;[47] the solver is also efficiently parallelized.

We have carefully benchmarked these calculations against both analytical and numerical benchmarks. Pressure drops were calculated with GeoDict for a number of test problems. These include Stokes flow past a single sphere,[48] settling of a sphere in a circular cylinder,[46] and flow past periodic arrays of spheres,[49] all of which were matched to within 1% of exact results. In flow through networks of up to 20 particles, GeoDict results were in excellent agreement with COMSOL[50] simulations. For production calculations in GeoDict, the primary particles were modeled as having $a = 4.95 \times 10^{-7}$ m, the fluid was modeled as air ($\mu = 1.834 \times 10^{-5}$ kg/m · s, $\rho = 1.204$ kg/m³), and a pressure drop of 0.02 Pa was imposed across the simulation cell. Permeability results were found to be

independent of variation of these parameters to six significant figures.

For each structure type and volume fraction, flow calculations were performed on five independently generated structures and the results were averaged. Uncertainties were calculated from the standard deviation as $\pm 2\sigma/\sqrt{5}$ and were below 1% for all $\phi > 0.005$. Uncertainties as high as ±5% were found at the lowest volume fractions $0.001 \leq \phi \leq 0.005$. This may indicate that yet larger simulation cells could be beneficial, but analyses below suggest that system size is not a serious issue. Mesh resolutions of between 2 and 16 lattice points per particle diameter were used in these calculations; at each ϕ, multiple system sizes and lattice resolutions were used to confirm that results were converged to within statistical uncertainty. Selected data from convergence studies and discretizations used in production calculations are given in the supplementary material.

Calculations were performed on four cores of a computer equipped with an Intel i7-7820X processor (3.60 GHz clock speed). The time required to complete one of these calculations varies in a complex way with both the grid size and the volume fraction; for lower volume fractions (and larger pores), the adaptive-grid solver works more efficiently, but larger simulation cells are required. For example, a single permeability calculation at $\phi = 0.002$ in a simulation cell measuring $1000a$ on each side with a discretization of $a/2$ (four points per diameter) required approximately 6 GB memory and was completed in approximately 2000 s. By contrast, at $\phi = 0.10$, boxes of only $40a$ edge length were necessary and well-converged calculations discretized at $a/8$ (sixteen points per diameter) spacing were completed in approximately 40 s and required around 0.25 GB memory.

IV. RESULTS

A. Pore size

We begin with the analysis of results for pore size and largest passable probe diameter (LPD). Figure 2 shows these
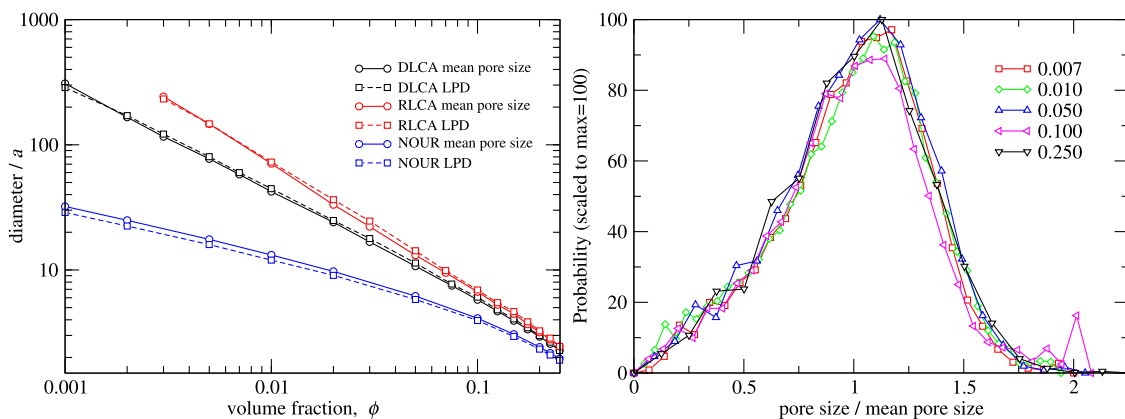
FIG. 2. Left: comparison of mean pore size and largest-passable probe diameter in DLCA, RLCA, and NOUR structures. Diameters are given in units of particle radius, a. Right: comparison of DLCA pore size distributions at varying ϕ, each scaled by the corresponding mean pore size.

quantities for the three classes of the model presented. The power-law dependence of DLCA and RLCA mean pore sizes at low volume fraction is clearly evident in this plot and is discussed below. RLCA structures have somewhat larger pores than DLCA structures; at $\phi = 0.01$, the mean RLCA pore size is 70.8, while the mean DLCA pore size is 42.2; the RLCA:DLCA ratio is thus 1.67:1. This ratio is not constant and grows as the volume fraction is reduced; at $\phi = 0.003$, it is 2.09:1. DLCA and RLCA structures have much larger pores than NOUR structures, which is due to their heterogeneous distribution of mass in the fractal regime. In both DLCA and RLCA, the LPD is very nearly the same as the mean pore size, which is somewhat surprising, while in NOUR structures, the LPD is 6.4% smaller than the mean pore size. Quantitatively, in DLCA, the LPD is 3.0% larger than the mean pore size, nearly independent of ϕ, while in RLCA, the LPD is 3.7% larger than the mean pore size, also almost independent of ϕ. In both cases, at the very lowest ϕ considered, the LPD is slightly smaller than the mean pore size. This is curious, but likely not very significant because the LPD is a statistically "noisy" quantity; in the data here, the uncertainty in LPD at low ϕ is around 4% relative.

A selection of DLCA pore size distributions (PSDs) are also shown in Fig. 2, each scaled by its mean. It is clear that the shape of the PSD is largely independent of ϕ, which is consistent with fractal behavior, though it is somewhat surprising that this behavior persists even to very high volume fractions. The standard deviation of the pore size relative to the mean, $\sigma_D/\overline{D}$, is approximately 0.33 in all cases. Inserting this into Eq. (16) suggests that polydispersity increases the permeability of these materials by about $0.33^2 \simeq 0.11$, or 11%; the assumption of monodispersity in theoretical models for permeability should therefore lead to systematic underprediction but only by a small amount, $\mathcal{O}(10\%)$.

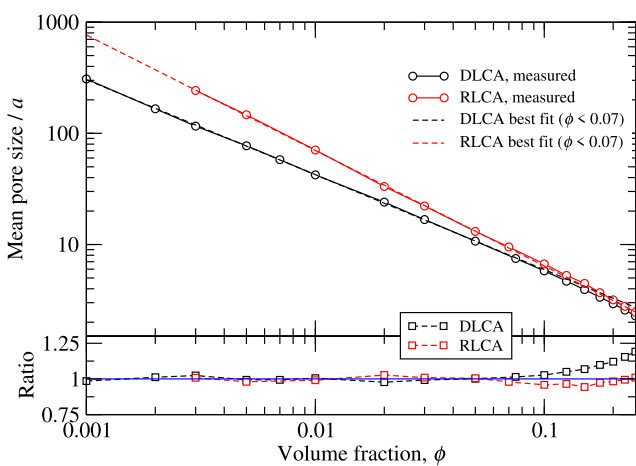Figure 3 again shows the DLCA and RLCA mean pore size data, along with power-law fits to data at $\phi < 0.07$. For both DLCA and RLCA, the mean pore size obeys power-law behavior from low volume fractions up to approximately this point, after which negative deviations are seen. The excellent fits to low-ϕ data suggest that, at least in regard to this structural measure, the simulation cells used are sufficiently large. Extrapolation of this power-law fit to high volume fraction overpredicts the DLCA mean pore size by as much as 20%; interestingly, the corresponding extrapolation for RLCA structures is nearly correct even to $\phi = 0.25$, with only some very small underpredictions made for ϕ around 0.1.

The power-law slope of the low-ϕ DLCA data is −0.854, which translates to a fractal dimension of $d_f = 1.830$, and that from the low-ϕ RLCA data is −1.038, which yields $d_f = 2.037$; these values are in reasonable agreement with previous simulation studies of DLCA and RLCA structures.[19,21,38,51] The corresponding prefactors are 0.831 for DLCA and 0.588 for RLCA.

These fractal dimensions are consistent with those obtained from radial distribution functions shown in Fig. 4. In aggregate materials, the radial distribution of particles around each other displays a characteristic shape, with a strong peak at the contact distance and short-ranged structure due to the non-overlap condition, followed by a power-law decay and, at sufficiently long distances, uniform behavior. In the fractal range, it is well-established[52] that $g(r) \propto r^{d_f - 3}$. Analysis of the data in Fig. 4 yields fractal dimensions of 1.85 for the DLCA structure and 2.06 for the RLCA structure, in good agreement with (though very slightly higher than) those obtained from fitting the mean pore size data in Fig. 3.

We now turn to the predictions of the different pore-size predictors discussed in Sec. II A: the Manley, cluster, and hydraulic models. In all three models, the fractal dimension is a parameter, and in the latter two one must also make a choice for ϕ_c, the cluster packing fraction. Figure 5 shows a comparison of the three predictions for DLCA structures made with $\phi_c = 0.40$ and $\phi_c = 0.50$ (note that for $\phi_c = 0.40$, the

FIG. 3. Top: best power-law fits to DLCA and RLCA mean pore size data at low volume fractions. Bottom: ratios of power-law predictions to measured pore sizes.
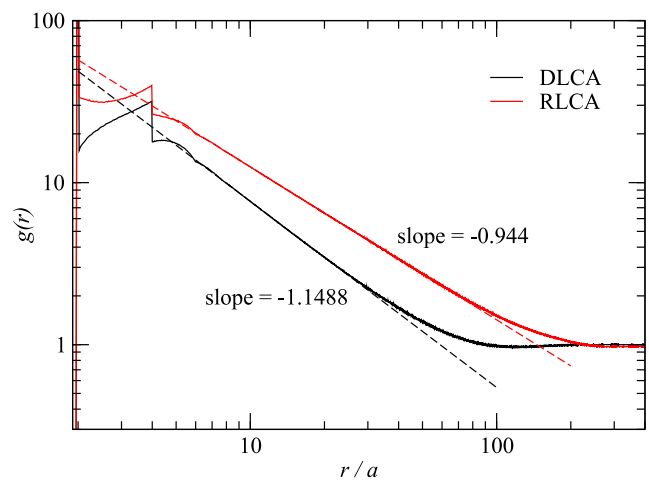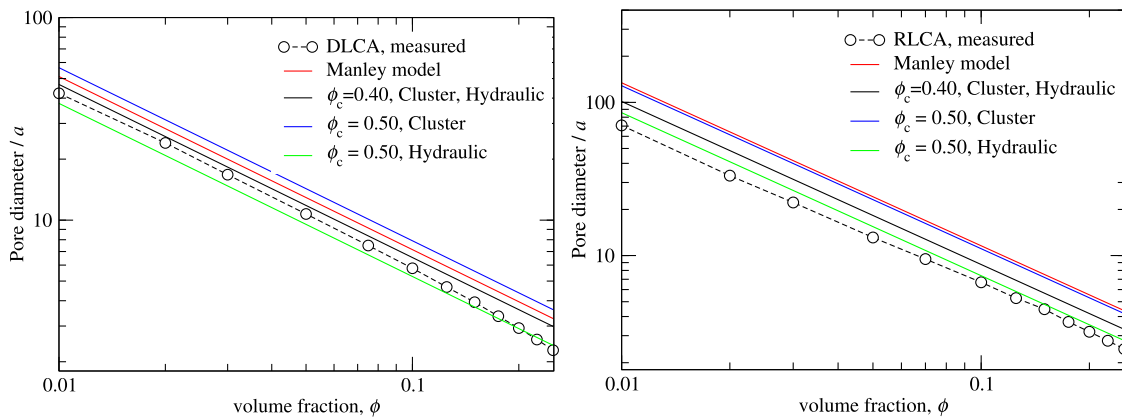

FIG. 4. Radial distributions from DLCA and RLCA models at volume fraction $\phi = 0.003$ and power-law fits to the fractal range of each.

FIG. 5. Predictions of different models for DLCA (left) and RLCA (right) mean pore sizes. At $\phi_c = 0.40$ the cluster and hydraulic models are identical.

cluster-model and hydraulic-model prefactors are equal). As the only difference between the models is the prefactor, their predictions are parallel lines on the log-log plot. We see that in the DLCA case, the Manley model slightly overpredicts the pore size, both cluster and hydraulic models overpredict at $\phi_c = 0.40$, while at $\phi_c = 0.50$, the cluster model overpredicts but the hydraulic model underpredicts. In the RLCA case, all the models overestimate pore size at these values of ϕ_c. The maximum low-ϕ overestimations are around 35% in the DLCA case and around 65% in the RLCA case.

None of the models capture the deviations from power-law behavior at high ϕ because they are based on the assumption of fractal cluster structure at all volume fractions. This assumption must break down at high ϕ when the cluster size becomes comparable with the particle size; if clusters contain only a few particles, then their internal structure cannot be truly self-similar at all length scales. This point is discussed further in Sec. IV B.

The reasonable agreement obtained in Fig. 5 and the modest dependence of the cluster and hydraulic model prefactors on choice of ϕ_c suggest that one could choose "optimal" values to exactly fit the pore size data, at least at low ϕ. These have been calculated and are shown in Table I. Unfortunately, little insight into the underlying physics is gained by this analysis. Different behavior is observed for DLCA and RLCA models and, while the ϕ_c values found are at least within a physically reasonable range, there is no obvious trend. Examination of the corresponding expressions [Eqs. (18) and (19)] shows that for the cluster model, the prefactor is an increasing function of ϕ_c, while for the hydraulic model the prefactor is a

decreasing function of ϕ_c. The different ϕ_c values required to match DLCA and RLCA data arise from the fact that the best-fit prefactor for RLCA is lower than that for DLCA; in the cluster model, this results in a lower ϕ_c for RLCA than for DLCA, while in the hydraulic model the converse is observed. In all cases, the best-fit ϕ_c values are rather lower than the random close-packing value of $\phi_c \simeq 0.64$, suggesting that within the framework of this model, one should think of the clusters as only loosely packed and thus connected to relatively few neighboring clusters.

B. Permeability

An example GeoDict flow velocity field in a $\phi = 0.005$ DLCA structure is visualized in Fig. 6. Although the fluid permeates the entire structure, there are clearly conduits of high flow rate that emerge as the low velocity regions near to the gel structure are masked. These are of irregular shape and varying diameter and exhibit branching and merging in a complex topology. This behavior is not accounted for in the expressions for permeability developed earlier, which assumed flow through independent cylindrical pores of unvarying diameter.

The permeabilities determined from flow simulations in DLCA, RLCA, and NOUR structures are shown in Fig. 7, along with predictions made using the measured pore size distributions and the PSD-averaged permeability expression of Eq. (15). In the case of DLCA and RLCA structures, power-law behavior is clearly observed at low volume fractions, with some negative deviations at high volume fractions; these will be discussed in greater detail below. Except in RLCA models at the very highest ϕ, the PSD-based predictions underpredict the permeability in all cases. In RLCA models, the PSD-based predictions are equal to approximately 0.8 times the true permeability for $\phi \leq 0.03$, independent of ϕ. At higher ϕ, the agreement with Stokes calculations improves, though at $\phi = 0.25$, the PSD-based prediction is slightly too high. In DLCA models, the PSD-based predictions are equal to approximately 0.55 times the true permeability for $\phi \leq 0.03$, also

TABLE I. Optimal choices of ϕ_c for model predictions of the low-ϕ mean pore size in DLCA and RLCA structures.

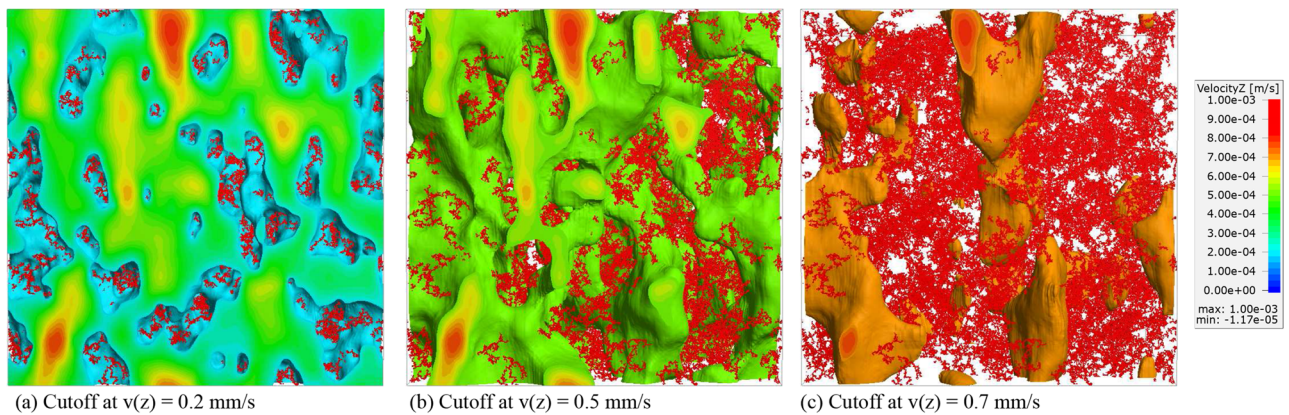| Model	ϕ_c^{PSD} (DLCA)	ϕ_c^{PSD} (RLCA)
Cluster	0.36	0.31
Hydraulic	0.44	0.55

(a) Cutoff at v(z) = 0.2 mm/s   (b) Cutoff at v(z) = 0.5 mm/s   (c) Cutoff at v(z) = 0.7 mm/s

FIG. 6. Stokes flow vertical velocity field in a ϕ = 0.005 DLCA structure (red), with three different cutoffs applied to remove the slowest-moving fractions. The flow direction is from the top to the bottom; the color scale is the same for all three visualizations.

independent of ϕ. As in the RLCA case, performance improves at higher ϕ, but does not ever reach quantitative agreement. In NOUR models, the PSD-based prediction substantially underestimates the true permeability at all ϕ, quite dramatically so at low ϕ.

The underprediction of permeability by the PSD-based calculation in all cases suggests that the pore size as measured by the spherical-probe insertion technique is smaller than the hydrodynamically relevant one. That is, the diameter of the channels through the gel that controls fluid transport is somewhat larger than the diameter of the largest spherical probe that can be moved through the network (which, recalling Fig. 2, is very nearly the same as the mean pore diameter as measured by the sphere-insertion method). The measured mean pore diameters were also generally smaller than the

FIG. 7. Top: Measured permeabilities and predictions based on the pore size distribution. Bottom: ratios of predicted to measured permeabilities for each type of structure. The statistical uncertainties in the measured permeabilities are smaller than the symbols used.

predictions of the cluster-size-based models, which suggests that fluid transport through the fractal clusters themselves contributes substantially to the overall permeability and also that the choice of $(1 - \phi)$ instead of $(1 - \phi_c)$ in accounting for porosity was the correct one. An alternative possibility for the discrepancy between simulated and PSD-predicted permeabilities is that variations in the pore shape or diameter lead to a higher net flow rate, which has been shown to occur in pores of sinusoidally varying diameter.[53]

Predictions of the various theories for gel permeability from Sec. II C are shown in Fig. 8. For the DLCA results, the power-law fit to the measured data at volume fractions $\phi < 0.05$ is $k_0/a^2 = 0.036\,84\phi^{-1.739}$, which corresponds to a fractal dimension of 1.85. This is in excellent agreement with the value obtained from the radial distribution function, but slightly higher than the 1.83 obtained from analysis of the mean pore size data.

As in the analysis of pore size, the cluster model and hydraulic model predictions depend on the choice of the cluster volume fraction ϕ_c. We first consider the DLCA results. In applying the Manley, cluster, and hydraulic models a fractal dimension of d_f = 1.85 was used. The Manley model greatly overestimates the permeability at all ϕ, by a factor of $1/0.036\,84 \simeq 27$. Taking ϕ_c = 0.5, the cluster model is essentially quantitative at low volume fractions but fails to capture the substantial negative deviation from fractal behavior at high ϕ; instead, it overpredicts high-ϕ permeabilities by as much as 300% at ϕ = 0.25. At ϕ_c = 0.5, the hydraulic model substantially underpredicts gel permeability, but at ϕ_c = 0.305 (not shown), it has the same prefactor as the cluster model and so performs equally well.

In the RLCA case, generally similar results are obtained. The best fit power-law at low volume fractions ($\phi \le 0.05$) is $k_0/a^2 = 0.013\,55\phi^{-2.122}$, which corresponds to a fractal dimension of d_f = 2.057, again in excellent agreement with that found from $g(r)$ data but slightly higher than that found from analysis of mean pore size data. In this case, at ϕ_c = 0.50, it is the
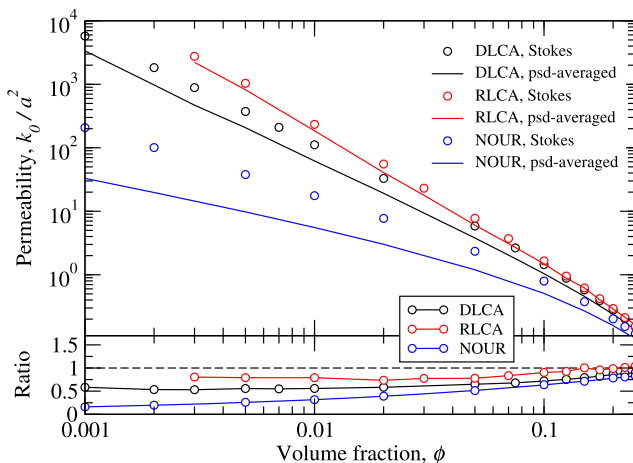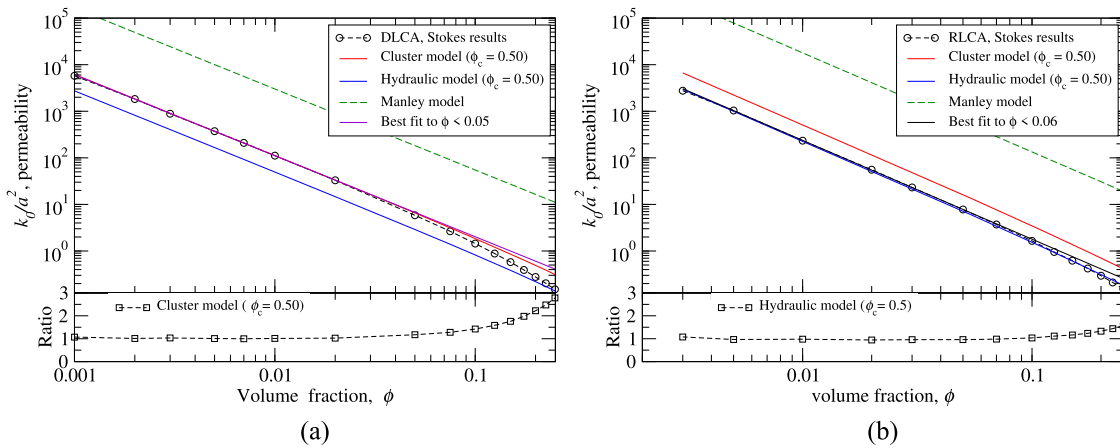
FIG. 8. Measured DLCA and RLCA permeabilities and predictions made using different theories from Sec. II C; no correction for polydispersity is applied. In each case, the ratio of the best theoretical prediction to the Stokes results is shown at bottom.

hydraulic model that is nearly quantitative at low ϕ and over-predicts at high ϕ, by as much as 1.5-fold at ϕ = 0.25. With ϕ_c = 0.50, the cluster model also overpredicts RLCA perme-abilities, but by reducing ϕ_c to 0.35, the cluster model has the same prefactor as the hydraulic model at ϕ_c = 0.5 and so performs equally well.

The ϕ_c values required to quantitatively match perme-ability data and pore size data do not agree for either DLCA or RLCA. For DLCA, the optimal value for permeability pre-diction with the cluster model is ϕ_c = 0.5, but is ϕ_c = 0.36 for pore-size prediction (Table I). The discrepancy is related to the underprediction of permeabilities in Fig. 7; larger pore sizes than were measured are necessary to match measured permeabilities, which in the case of the cluster model trans-lates to higher optimal ϕ_c values. In the RLCA case, a sim-ilar trend is observed. In the case of the hydraulic models, lower ϕ_c values are required to match measured permeabili-ties than pore sizes in both the DLCA and RLCA cases, again because the prefactor is a decreasing function of ϕ_c in that model.

In both cluster-model and hydraulic-model predictions, there is a small deviation from power-law scaling visible at high ϕ, which is due to the $1 - \phi$ term that results from porosity considerations as discussed earlier. Although in the right direction, this is clearly insufficient to account for the observed behavior of the measured permeability. A possible explanation for this is that the fractal dimension is itself a function of ϕ, at least at high ϕ. Such a variation was proposed by Lach-hab et al., who studied the variation of aggregate radii of gyration with size during on-lattice DLCA and RLCA sim-ulations, that is, before gelation.[51] Considering only clusters of size N > 50, they estimated the fractal dimensions in each case using Eq. (1). They found that DLCA fractal dimensions measured in this way were well fit by d_f = 1.80 + 0.91$\phi^{0.51}$, and RLCA fractal dimension data were well fit by d_f = 2.10 + 0.47$\phi^{0.66}$. Substitution of these results into any of our

preceding models for permeability does not yield satisfactory results. However, taking $d_f = d_f{}^0 + a\phi^b$, where $d_f{}^0$ is the low-ϕ fractal dimensions obtained from $g(r)$ analysis, and treating a and b as adjustable parameters does lead to excellent fits of the Stokes permeability data, as shown in Fig. 9.

Only the cluster model was used in this analysis. The best fit in the DLCA case has d_f = 1.85 + 0.2$\phi^{0.25}$ and ϕ_c = 0.30. The best fit in the RLCA case has d_f = 2.06 + 0.4$\phi^{0.5}$ and ϕ_c = 0.30 again. In both cases, the maximum unsigned relative deviation from the Stokes results is below 10% over the entire range of ϕ studied. The dependences of d_f on ϕ obtained from this analysis are similar but not identical to those of Lach-hab et al.[51] One possible source of this discrepancy is the dif-ference between on-lattice and off-lattice models and small
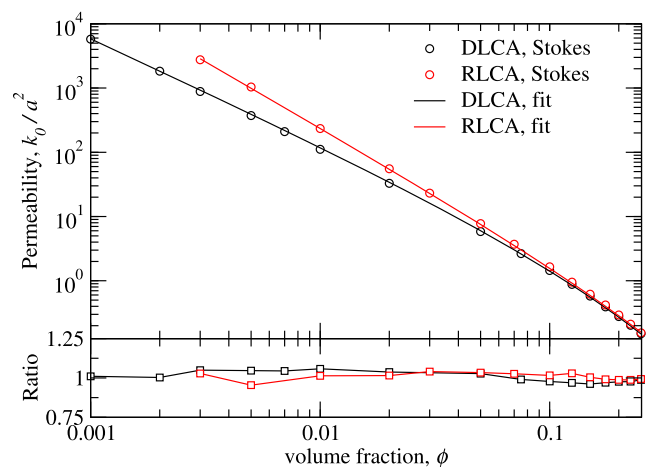
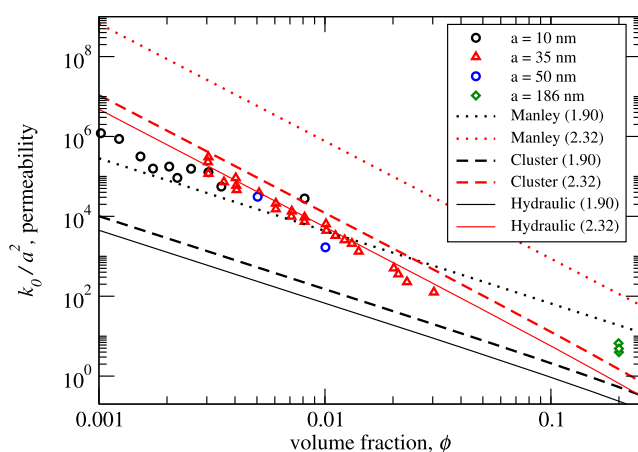

FIG. 9. Measured permeabilities and predictions made using ϕ-dependent d_f values in the cluster model. The lower graph shows the ratios of predicted to measured permeabilities for each type of structure.

differences in the simulation algorithms used. Another issue is that these fits are made using permeability models based on a number of approximations, which may lead to systematically different effective d_f values at high volume fractions. Finally, the relevant cluster size for the determination of pore size in gels at higher volume fractions is likely smaller than the N > 50 criterion used by Lach-hab et al. Combining Eqs. (1) and (6) yields $N_c = (\phi_c/\phi)^{d_f/(3-d_f)}$. For $\phi_c = 0.5$ and $\phi = 0.1$, this predicts that DLCA clusters contain only about $N_c = 12.3$ particles; at $\phi = 0.05$ where deviations from power-law behavior are only just visible, one gets $N_c = 36.3$. It is possible, therefore, that permeability measurements and the analysis of Lach-hab et al. are probing two different length scales. Note that it is not possible to use the $g(r)$ analysis (viz., Fig. 4) to resolve this question because at high ϕ the range of fractal behavior is very short and obscured by short-range packing effects.

C. Application to experimental data

There are relatively little data on gel permeability in the literature; what are available were collected by Manley et al.[23] and are reproduced here in Fig. 10, along with various analyses. The two data sets with a = 10 nm and a = 50 nm were measured by Manley et al. and were claimed to be DLCA-like, with fractal dimension near 1.9. The a = 35 nm data set was obtained by Allain et al.[27] who extracted a fractal dimension of 2.32 from their data, consistent with a subsequent determination of 2.2 ± 0.1 measured from the settling velocities of individual aggregates with sizes determined by microscopy.[54] The final data set (a = 168 nm) was obtained by Starrs et al., who did not measure a fractal dimension.[28] No information concerning statistical uncertainty is available for these data sets. We found that the scatter around separate power-law fits to the a = 10 nm data and a = 35 nm data is in each

FIG. 10. Theoretical predictions for experimental permeabilities. Symbols represent experimental data points; the a = 10 nm and a = 50 nm data were measured by Manley et al.,[23] a = 35 nm data were measured by Allain et al.,[27] and a = 186 nm data were measured by Starrs et al.[28] For each model prediction, the assumed fractal dimension is given in parentheses. $\phi_c = 0.50$ was used in both cluster model and hydraulic model predictions.

case contained within a range from 0.5× to 2.0× of the fit prediction; that is, the individual permeability measurements appear to be accurate only to within a factor of two. Manley et al. plotted all these data together and claimed that their model [Eq. (17)] with d_f = 1.9 (dashed black line in Fig. 10) adequately described the permeability over this entire range of ϕ, without mentioning the substantially different d_f of the data set of Allain et al.

In fact, the Manley model with d_f = 2.32 (red dashed line) greatly overpredicts all of the corresponding experimental data, though has the correct slope for the a = 35 nm data set. The hydraulic model, with d_f = 2.32 and ϕ_c = 0.5, is in excellent agreement with the a = 35 nm data and clearly shows that the data of Allain et al. can be much better fit by a model with d_f = 2.32 than the one with d_f = 1.9 (dashed black line). The cluster model with the same parameters modestly overpredicts the experimental data, but, as above, modest adjustment of ϕ_c would achieve the same result as with the hydraulic model. These results are consistent with the good performance of the hydraulic model (with ϕ_c = 0.5) for simulated RLCA structures with d_f = 2.06. However, the cluster and hydraulic models with d_f = 1.9 both underpredict the measurements of Manley et al. by nearly two orders of magnitude. Recall that the cluster model was nearly quantitative for the simulated DLCA (d_f = 1.85) permeabilities in Fig. 8, while the hydraulic model was off by a factor of only approximately 0.5. There is no obvious explanation for the poor agreement of the model predictions for absolute permeability with the data of Manley et al. Finally, none of the predictions come within better than a factor of 10 of the data of Starrs et al. Since d_f is not available for this data set, it is not even clear which model should be closer; both the hydraulic and cluster predictions are too low, while the predictions of the Manley model are too high. We also note that a best-fit line through the a = 10 nm and a = 50 nm data with the slope corresponding to d_f = 1.9 will overpredict the data of Starrs et al. by an even greater amount (not shown.)

V. CONCLUSIONS

In this work, we used simulated gel-like structures and first-principles fluid mechanical calculations to study the relationships between the gel structure and permeability. Both DLCA and RLCA materials were studied in depth, with some additional comparisons made to NOUR structures. Simulations of very large systems and averaging over many independent realizations were used to obtain data of high quality. Scaling relations developed in previous studies[14,23,27] were reanalyzed and refined in order to obtain accurate models for the variation of permeability with volume fraction. Geometrical analyses were used to extract pore size distributions, largest-passable probe diameters, and fractal dimensions for use in property predictions and interpretations.

Theoretical predictions based on the fractal cluster model were found to be in good agreement with simulated pore size and permeability data for volume fractions up to approximately ϕ = 0.07 (pore size) and ϕ = 0.05 (permeability),

with negative deviations seen for both quantities at higher ϕ. At ϕ = 0.25, the highest studied, the permeability of DLCA structures was approximately 1/3 of the value predicted, while the permeability of RLCA structures was approximately 70% of the value predicted. That is, power-law behavior persists to higher ϕ for RLCA than DLCA, which is likely due to the larger pore and cluster sizes in RLCA.

Fractal dimensions extracted from mean pore size data and radial distribution functions are in good, but not perfect, agreement, with pore-size d_f results slightly smaller than those obtained from $g(r)$. This is not unexpected; colloidal gels are only fractal over a certain range of length scales, and different methods for estimating d_f probe these length scales somewhat differently.

Three separate models for predicting pore size and permeability were considered; the "Manley" model,[23] the "cluster" model, and the "hydraulic" model. The cluster and hydraulic model predictions differ only in prefactor, though the prefactor is itself dependent (weakly) on the fractal dimension. All three pore-size models agree to within a factor of about 3 for reasonable choices of the cluster volume fraction ϕ_c, which is an input parameter. The cluster and hydraulic models for permeability contain a porosity-related factor of $1 - \phi$ which provides for some negative deviation from power-law scaling at high ϕ, but not enough to completely account for the observed deviations. The Manley model omits a factor of 1/32 that arises from the Hagen-Poiseulle result for flow in a cylinder and as a result substantially overestimates the permeability of both DLCA and RLCA simulated structures. The cluster and hydraulic models retain this term and give permeabilities quite close to the simulated values. These models can be made to give quantitative agreement with both DLCA and RLCA simulation results at low ϕ through choice of the ϕ_c parameter. The necessary ϕ_c values are not transferable between DLCA and RLCA, and the optimal values of ϕ_c for the cluster model and hydraulic model are themselves different in each case, but the generally low values of ϕ_c required suggest that the packing of clusters is relatively low-coordination. Nonetheless, even just taking $\phi_c = 0.5$ in all cases, the model predictions for permeability are within a factor of three of the simulated values over the entire ϕ range studied. Predictions of permeability made using the measured pore size distributions were systematically low, indicating that the pore size as measured by spherical-probe insertion is smaller than the hydrodynamically relevant pore size in these materials; this was true even for NOUR structures.

Analysis of pore size distributions suggests that polydispersity in pore size does not have a substantial effect on permeability in DLCA and RLCA structures, with the caveat that this does not consider variation in diameter along the length of a single pore. Nonetheless, the effects of such variations, along with reductions in permeability due to "tortuosity" of high-flow channels, cannot be very large, given the reasonable agreement obtained when excluding them. A more promising way to account for deviations from power-law behavior

at high ϕ is to model the fractal dimension of the materials as weakly dependent on ϕ. Excellent empirical fits of the permeability over the entire ϕ range studied can thus be obtained. However, the variation of d_f with ϕ thus obtained differs from previous literature results,[51] and it is not clear if it is possible to determine the necessary parameters from analysis of the model structures.

Finally, comparison of the proposed models with available experimental data yielded mixed results. Both the hydraulic and cluster models were found to agree well with the data of Allain *et al.*,[27] but were very far from the data of Manley *et al.* Conversely, the Manley model prediction was quite close to their own data, but failed badly for both the simulated results and the data of Allain *et al.* when the correct fractal dimensions were input. This discrepancy cannot be resolved without further experimental work, though one can speculate as to possible causes. One possibility would be some pre-aggregation of particles prior to the gelation experiments by Manley *et al.* This would lead to an effective particle radius a which is much larger than that of primary particle a and thus to an overestimation of k_0/a^2.

From an empirical standpoint, it appears that fitting a power-law dependence to low-ϕ data will give good results for volume fractions up to around 0.05-0.10, with modest over-predictions at higher ϕ; furthermore, deviations from power-law behavior seem to be smaller for materials with higher fractal dimension. The models discussed in this work involve a considerable number of simplifying approximations and at least one parameter (ϕ_c) difficult to assign *a priori*, yet give generally good, though not exact results, especially at high ϕ. It is plausible that ϕ_c could be determined by further geometric analysis of the gel structure and/or gelation simulation trajectories (or by experiment), but this has not been attempted. The inclusion of ϕ-dependent fractal dimension is sufficient to obtain quantitative results, but that dependence itself is not widely studied and such data are rarely available. Finally, the RLCA and DLCA structures studied here are "limiting cases" in the sense that the underlying simulations permit no relaxation or spinodal-type coarsening of the gel structure as it forms; the performance of the various models in these systems may therefore not be transferable to (experimental or simulated) systems which do display such behaviors. First-principles prediction of the absolute permeability of fractal gel networks therefore remains a challenging problem.

SUPPLEMENTARY MATERIAL

See supplementary material for the system sizes and discretization parameters used in production calculations, as well as selected data from GeoDict convergence studies.

ACKNOWLEDGMENTS

engineering sciences. Through his mentorship, textbooks, and publications, he introduced many of us to the fundamentals of molecular theory and the transport of heat, mass, and momentum. Here we have applied some these insights to better understand the interrelationship between the structure of colloidal networks and how fluids flow through them. We gratefully acknowledge Professor Bird's contributions to both the sciences and ourselves on the occasion of his 95th birthday and wish him many happy returns.

REFERENCES

[1] P. J. Lu and D. A. Weitz, "Colloidal particles: Crystals, glasses, and gels," Annu. Rev. Condens. Matter Phys. **4**, 217–233 (2013).

[2] D. H. Everett, *Basic Principles of Colloid Science* (Royal Society of Chemistry, 2007).

[3] P. Burey, B. R. Bhandari, T. Howes, and M. J. Gidley, "Hydrocolloid gel particles: Formation, characterization, and application," Crit. Rev. Food Sci. Nutr. **48**, 361–377 (2008).

[4] Q. Wang, L. Wang, M. S. Detamore, and C. Berkland, "Biodegradable colloidal gels as moldable tissue engineering scaffolds," Adv. Mater. **20**, 236–239 (2008).

[5] M. J. Murray and M. J. Snowden, "The preparation, characterisation and applications of colloidal microgels," Adv. Colloid Interface Sci. **54**, 73–91 (1995).

[6] N. Gaponik, A.-K. Herrmann, and A. Eychmuller, "Colloidal nanocrystal-based gels and aerogels: Material aspects and application perspectives," J. Phys. Chem. Lett. **3**, 8–17 (2012).

[7] T. Cosgrove, *Colloid Science: Principles, Methods and Applications* (John Wiley & Sons, 2010).

[8] M. Guvendiren, H. D. Lu, and J. A. Burdick, "Shear-thinning hydrogels for biomedical applications," Soft Matter **8**, 260–272 (2012).

[9] A. O. Barel, M. Paye, and H. I. Maibach, *Handbook of Cosmetic Science and Technology* (CRC Press, 2014).

[10] J. L. Knowlton and S. E. M. Pearce, *Handbook of Cosmetic Science and Technology* (Elsevier, 2013).

[11] D. A. Weitz and M. Oliveira, "Fractal structures formed by kinetic aggregation of aqueous gold colloids," Phys. Rev. Lett. **52**, 1433 (1984).

[12] L. C. Hsiao, R. S. Newman, S. C. Glotzer, and M. J. Solomon, "Role of isostaticity and load-bearing microstructure in the elasticity of yielded colloidal gels," Proc. Natl. Acad. Sci. U. S. A. **109**, 16029–16034 (2012).

[13] E. Zaccarelli, "Colloidal gels: Equilibrium and non-equilibrium routes," J. Phys.: Condens. Matter **19**, 323101 (2007).

[14] M. Carpineti and M. Giglio, "Spinodal-type dynamics in fractal aggregation of colloidal clusters," Phys. Rev. Lett. **68**, 3327–3330 (1992).

[15] L. C. Hsiao, H. Kang, K. H. Ahn, and M. J. Solomon, "Role of shear-induced dynamical heterogeneity in the nonlinear rheology of colloidal gels," Soft Matter **10**, 9254–9259 (2014).

[16] P. Meakin, "Formation of fractal clusters and networks by irreversible diffusion-limited aggregation," Phys. Rev. Lett. **51**, 1119–1122 (1983).

[17] M. Y. Lin, H. M. Linday, D. A. Weitz, R. Klein, R. C. Ball, and P. Meakin, "Universal diffusion-limited colloid aggregation," J. Phys.: Condens. Matter **2**, 3093–3113 (1990).

[18] W. C. K. Poon and M. D. Haw, "Mesoscopic structure formation in colloidal aggregation and gelation," Adv. Colloid Interface Sci. **73**, 71–126 (1997).

[19] P. Meakin, "A historical introduction to computer models for fractal aggregates," J. Sol-Gel Sci. Technol. **15**, 97–117 (1999).

[20] A. Hasmy, M. Foret, J. Pelous, and R. Jullien, "Small-angle neutron-scattering investigation of short-range correlations in fractal aerogels - Simulations and experiments," Phys. Rev. B **48**, 9345–9353 (1993).

[21] A. Hasmy, E. Anglaret, M. Foret, J. Pelous, and R. Jullien, "Small-angle neutron-scattering investigation of long-range correlations in silica aerogels - simulations and experiments," Phys. Rev. B **50**, 6006–6016 (1994).

[22] H.-S. Ma, J.-H. Prévost, R. Jullien, and G. W. Scherer, "Computer simulation of mechanical structure-property relationship of aerogels," J. Non-Cryst. Solids **285**, 216–221 (2001).

[23] S. Manley, J. M. Skotheim, L. Mahadevan, and D. A. Weitz, "Gravitational collapse of colloidal gels," Phys. Rev. Lett. **94**, 218304 (2005).

[24] R. Buscall, T. H. Choudhury, M. A. Faers, J. W. Goodwin, P. A. Luckham, and S. J. Partridge, "Towards rationalising collapse times for the delayed sedimentation of weakly-aggregated colloidal gels," Soft Matter **5**, 1345 (2009).

[25] S. B. Lindström, T. E. Kodger, J. Sprakel, and D. A. Weitz, "Structures, stresses, and fluctuations in the delayed failure of colloidal gels." Soft Matter **8**, 3657 (2012).

[26] J. Sprakel, S. Lindström, T. Kodger, and D. Weitz, "Stress enhancement in the delayed yielding of colloidal gels," Phys. Rev. Lett. **106**, 248303 (2011).

[27] C. Allain, M. Cloitre, and M. Wafra, "Aggregation and sedimentation in colloidal suspensions," Phys. Rev. Lett. **74**, 1478–1481 (1995).

[28] L. Starrs, W. C. K. Poon, D. J. Hibberd, and M. M. Robbins, "Collapse of transient gels in colloid-polymer mixtures," J. Phys.: Condens. Matter **14**, 2485–2505 (2002).

[29] F. A. L. Dullien, *Porous Media: Fluid Transport and Pore Structure*, 2nd ed. (Academic Press, Inc., San Diego, 1992).

[30] S. Bryant and M. Blunt, "Prediction of relative permeability in simple porous media," Phys. Rev. A **46**, 2004 (1992).

[31] S. Bryant, C. Cade, and D. Mellor, "Permeability prediction from geologic models," AAPG Bull. **77**, 1338–1350 (1993).

[32] M. Oda, "Permeability tensor for discontinuous rock masses," Geotechnique **35**, 483–495 (1985).

[33] M. D. Zoback and J. D. Byerlee, "Permeability and effective stress: Geologic notes," AAPG Bull. **59**, 154–158 (1975).

[34] S. J. Pirson, *Oil Reservoir Engineering* (RE Krieger Publishing Company, 1977).

[35] C. W. Fetter, *Applied Hydrogeology* (Prentice Hall, 2000).

[36] B. D. Hames, *Gel Electrophoresis of Proteins: A Practical Approach* (OUP Oxford, 1998), Vol. 197.

[37] G. K. Ackers, "Analytical gel chromatography of proteins," Adv. Protein Chem. **24**, 343–446 (1970).

[38] R. Jullien and R. Botet, *Aggregation and Fractal Aggregates* (World Scientific Pub. Co., Singapore, 1987).

[39] L. D. Gelb, "Simulation and modeling of aerogels using atomistic and mesoscale methods," in *Aerogels Handbook*, edited by M. A. Aegerter, N. Leventis, M. M. Koebel, and S. Steiner (Springer, New York, in press).

[40] R. Salazar and L. D. Gelb, "An investigation of the effects of the structure of gel materials on their adsorptive properties using a simple lattice-gas model," Mol. Phys. **102**, 1015–1030 (2004).

[41] R. Salazar and L. D. Gelb, "A computational study of the reconstruction of amorphous mesoporous materials from gas adsorption isotherms and structure factors via evolutionary optimization," Langmuir **23**, 530–541 (2007).

[42] L. D. Gelb and K. E. Gubbins, "Pore size distributions in porous glasses: A computer simulation study," Langmuir **15**, 305–308 (1999).

[43] M. Whittle and E. Dickinson, "Pore size in model particle gels," Mol. Phys. **96**, 259–264 (1999).

[44] Math2Market, Geodict software, version 2018, https://www.math2market.com.

[45] M. P. Allen and D. J. Tildesley, *Computer Simulation of Liquids* (Clarendon Press, Oxford, 1987).

[46] J. Happel and H. Brenner, *Low Reynolds Number Hydrodynamics: With Special Applications to Particulate Media* (Springer, 1991), Vol. 1.

[47]S. Linden, A. Wiegmann, and H. Hagen, "The LIR space partitioning system applied to the Stokes equations," Graph. Models **82**, 58–66 (2015).

[48]G. G. Stokes, "On the effect of the internal friction of fluids on the motion of pendulums," Trans. Cambridge Phil. Soc. **9**, 8 (1851).

[49]A. S. Sangani and A. Acrivos, "Slow flow through a periodic array of spheres," Int. J. Multiphase Flow **8**, 343 (1982).

[50]COMSOL Multiphysics version 5.2, www.comsol.com, COMSOL AB, Stockholm, Sweden, 2015.

[51]M. Lach-hab, A. E. González, and E. Blaisten-Barojas, "Concentration dependence of structural and dynamical quantities in colloidal aggregation: Computer simulations," Phys. Rev. E **54**, 5456–5462 (1996).

[52]M. Lattuada, H. Wu, A. Hasmy, and M. Morbidelli, "Estimation of fractal dimension in colloidal gels," Langmuir **19**, 6312–6316 (2003).

[53]M. Hemmat and A. Borhan, "Creeping flow through sinusoidally constricted capillaries," Phys. Fluids **7**, 2111–2121 (1995).

[54]C. Allain, M. Cloitre, and F. Parisse, "Settling by cluster deposition in aggregating colloidal suspensions," J. Colloid Surf. Sci. **178**, 411–416 (1996).